

Supporting Information:

High-Performance Iron Oxide Nanoparticles for Magnetic Particle Imaging – Guided Hyperthermia (hMPI)

Lisa M. Bauer,^{‡a} Shu F. Situ,^{‡b} Mark A. Griswold,^{*a,c} and Anna Cristina S. Samia^{*b}

^aDepartment of Physics, ^bDepartment of Chemistry, ^cDepartment of Radiology, Case Western Reserve University and University Hospitals of Cleveland, 11100 Euclid Avenue, Cleveland, OH 44106, USA.

† Denotes equal contribution.

1. EXPERIMENTAL METHODS

1.1. Materials and Reagents. Iron (III) chloride hexahydrate (98%), iron (III) acetylacetone (99%), zinc acetylacetone hydrate, zinc (II) chloride anhydrous (98%), 4-biphenylcarboxylic acid (95%), oleic acid (90%), oleylamine (70%), dioctyl ether (99%), 1-octadecene (90%), benzyl ether (98%), toluene, trimethylamine *N*-oxide (98%), and ultra-high molecular weight polyethylene (MW 3,000,000 – 6,000,000 g/mol) were purchased from Sigma-Aldrich and used as received. Hexane, sodium oleate, and ethyl alcohol were purchased from Fisher Scientific and were used without further purification steps.

1.2. Nanoparticle Synthesis and Nanocomposite Fabrication. Magnetic nanoparticles were prepared by modified thermal decomposition method based on procedures reported in previous literatures.¹⁻³ The nanoparticles were subsequently dispersed in toluene and incorporated into an ultra-high molecular weight polyethylene (UHMWPE) matrix using a compression molding approach. Nanoparticles dispersed in toluene were prepared with equal iron concentration for magnetic particle relaxometry and hyperthermia measurements.

1.2.1. Synthesis of Magnetite (Fe_3O_4) Spherical NP. Fe_3O_4 nanoparticles were synthesized in a two-step process involving the thermal decomposition of an iron oleate complex to form wüstite (FeO) nanoparticles followed by a mild oxidation step to obtain the Fe_3O_4 phase. The iron oleate precursor was prepared by dissolving iron (III) chloride hexahydrate ($FeCl_3 \cdot 6H_2O$, 40 mmol) and sodium oleate (120 mmol) in a solvent mixture containing deionized (DI) water (60 mL), ethanol (80 mL), and hexane (140 mL). The reaction mixture was heated at reflux for 4 h. After reflux, the organic layer containing the iron oleate precursor was separated from the aqueous layer and washed multiple times with warm water to remove salt by-products and excess reagents. Following the wash steps, the iron oleate mixture was dried under vacuum (762 mm Hg) for 72 h.

In a typical synthesis for magnetite nanoparticles with an average diameter of 18 nm, iron oleate (3.6 g), oleic acid (4.2 mL), and 1-octadecene (12 mL) were vigorously stirred under argon (Ar) atmosphere. The solution was then heated to 100 °C for 1 h, after which the temperature of the reaction mixture was slowly increased (3 °C/min) to 320 °C to reflux for an additional hour. The reaction mixture was then cooled to room temperature and the obtained FeO nanoparticles were precipitated out by centrifugation for 20 min at 7000 rpm using a 1:1 ethanol: toluene solvent mixture (30 mL). The FeO nanoparticles were further converted to Fe_3O_4 using trimethylamine *N*-oxide [$(CH_3)_3NO$] as oxidizing agent. More specifically, $(CH_3)_3NO$ (0.5 mmol) was added to FeO nanoparticles (400 mg) dispersed in 1-octadecene (20 mL) and the reaction mixture was first heated to 130 °C and held for 1 h, after which the reaction temperature was raised to 280 °C at a rate of 10 °C /min and held at that temperature for 1 h. The resultant Fe_3O_4 nanoparticles were isolated by the addition of a 1:1 ethanol: toluene solvent mixture (30 mL) and subsequent centrifugation for 20 min at 7000 rpm.

1.2.2. Synthesis of Magnetite (Fe_3O_4) Cubic NP. To synthesize Fe_3O_4 nanocubes with average 15 nm edge length, $Fe(acac)_3$, 4-biphenylcarboxylic acid, oleic acid and benzyl ether were stirred in 50 mL round bottom flask at 70 °C for 1 hr under Ar atmosphere and heated to 280 °C and maintained under reflux for 2 hrs.

1.2.3. Synthesis of Zinc-Doped Magnetite Spherical NPs. The zinc doped magnetite nanospheres were synthesized using $Fe(acac)_3$, $ZnCl_2$, oleic acid, oleylamine, and dioctyl ether. The reaction mixture was first mixed in 100 °C under Ar atmosphere for 1 hr. The temperature of reaction mixture was subsequently increased to 320 °C and refluxed for 1 hr.

1.2.4. Synthesis of Zinc-Doped Magnetite Cubic NPs. The synthesis procedure for zinc doped magnetite nanocubes was similar to the procedure for magnetite nanocubes reported in 1.2.3 with $Fe(acac)_3$ and $Zn(acac)_2$ as precursors.

1.2.5. Nanocomposite (NC) Fabrication. The NC was fabricated by a liquid-solid compounding method with 10 % w/w zinc-doped magnetite cubic NPs in ultra-high molecular-weight polyethylene using *p*-xylene as solvent. The dispersions were mixed in sonic bath for 4 h at room temperature, followed by vacuum drying overnight. To prepare the nanocomposite films, the resulting dried powder mixtures (0.5 g) were placed in an aluminum mold (1" in diameter and 1/32" thickness) that rested in between two iron steel plates and pressed using a Carver Model C laboratory press at a temperature of 200 °C under 10 metric ton of applied pressure for 20 min. The compressed NC films were then cut into small pieces (1 mm x 3 mm) and placed inside the 3-D printed multi-welled sample holder.

1.3. IONP Structural Characterization. The IONP size and shape were evaluated by transmission electron microscopy (TEM). TEM samples were prepared by placing 5 μ L of a dilute suspension of the MNPs on a 400 mesh Formvar-coated copper grid and allowing the

solvent to evaporate slowly at room temperature. TEM images were obtained with a FEI Tecnai G2 Spirit BioTWIN transmission electron microscope operated at 120 kV. The mean particle size and size distribution were evaluated by measuring at least 200 nanoparticles for each sample. The crystal structure of the samples was identified by powder x-ray diffractometry (XRD) performed in a Rigaku MiniFlex powder x-ray diffractometer using Cu-K α radiation ($\lambda=0.154$ nm). For the XRD analysis, the diffraction patterns were collected within a 2θ range of 25 to 75 °. The total Fe concentration in each sample was measured using a fast sequential atomic absorption spectrophotometer (AAS) Varian 220FS AA. For the elemental Fe analysis, the samples were digested with concentrated hydrochloric acid overnight to completely dissolve the IONPs.

1.3.1. Nanoparticle volume calculation. The volume of nanoparticles were calculated using the average diameter of spherical NPs and the edge length of cubic NPs estimated from the TEM measurement. The following formulas were used for the calculations:

Spherical NPs:

$$V_{Sphere} = \frac{4}{3}\pi r^3$$

r = radius of the sphere (half of sphere diameter)

Cubic NPs:

$$V_{Cube} = l^3$$

l = edge length of cube

1.4 Magnetic Particle Relaxometer and PSF Reconstruction. Magnetic particle relaxometry measures the one-dimensional PSF of a tracer. The relaxometer generates an excitation field that is analogous to the FFR sweeping back-and-forth over the sample under test. This signal is inductively detected and gridded to the (known) instantaneous magnetic field value to create the

PSF. The signal chain, depicted in Figure S2, is as follows: A sinusoidal signal ($f_0=16.8$ kHz) is fed to an audio power amplifier, and low-pass filtered to remove non- f_0 content. This generates a magnetic field of amplitude 20 mT at the sample. The signal from the tracers is detected by a receive coil, then notch filtered to remove f_0 feedthrough and amplified by a low-noise preamplifier, before being sampled at 500 ksps. A measurement of one sample takes approximately 30 seconds. The gridding process for reconstruction is depicted in Figure S3.

1.5 Magnetic Hyperthermia Measurements

The magnetic hyperthermia measurements were performed using an MSI Automation bench mount magnetic induction heating system. The IONP samples were exposed to an alternating magnetic field excitation at a fixed frequency (f) of 380 kHz and magnetic field amplitude (H) of 16 kA/m (the field strength was chosen to match the amplitude of the magnetic particle relaxometry excitation).

1.6 Magnetic Hyperthermia Measurements under a Static Magnetic Field

To test hyperthermia performance of tracers under a static magnetic field, the standard hyperthermia setup was modified by placing a single strong permanent magnet at varying distances (5.5-10 cm) from the coil.

1.7 Magnetic Hyperthermia Measurements under a Gradient Magnetic Field

To evaluate the magnetic hyperthermia performance under a gradient magnetic field, two strong permanent magnets were placed on both sides of the hyperthermia heat induction coil during the measurement. The magnets were arranged such that there was a 0.47T/m gradient across the hyperthermia coil with a null point near the center. A multi-well holder was custom designed and 3-D printed in ABS for this study. Small strips (1 mm x 3 mm) of polyethylene composite films containing zinc-doped magnetite cubic NPs were placed inside individual wells to

minimize thermal conductivity. A thermal camera (Seek Thermal Compact for Android) was used to visualize heating. The overall temperature change of nanocomposite strips after 30 sec of magnetic hyperthermia exposure was measured in the presence and absence of gradient magnetic field. A thermal image was recorded every 5 sec. The thermal images were processed in MatLab to obtain the image intensity profile of the line through the center of the multi-well holder. One may note that the image intensity profile is flat across each peak in the image without a gradient magnetic field; this is due to image saturation due to strong heating.

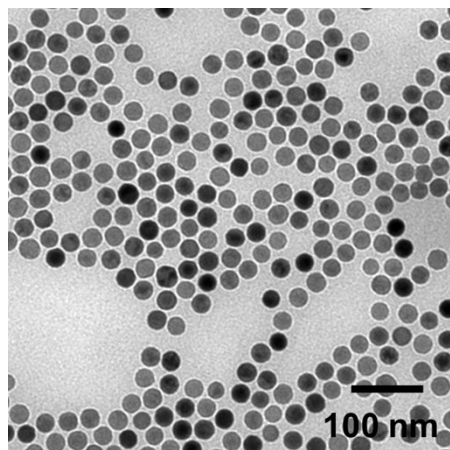


Figure S1. Transmission electron microscopy (TEM) image of commercially available MPI iron oxide nanoparticle tracer (Senior Scientific PrecisionMRX™ 25 nm oleic acid-coated).

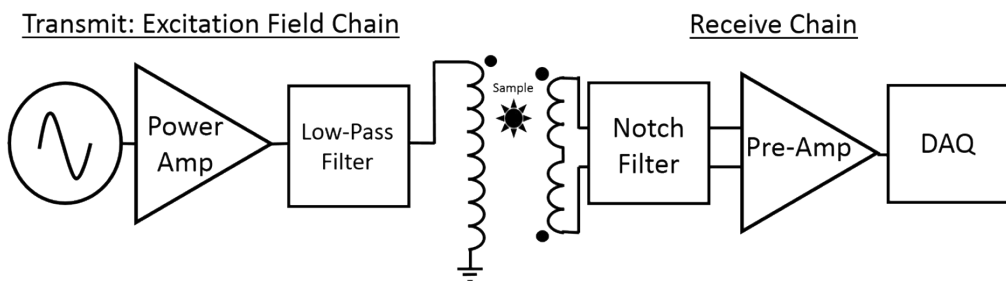


Figure S2. Overview of the x-space magnetic particle relaxometer.

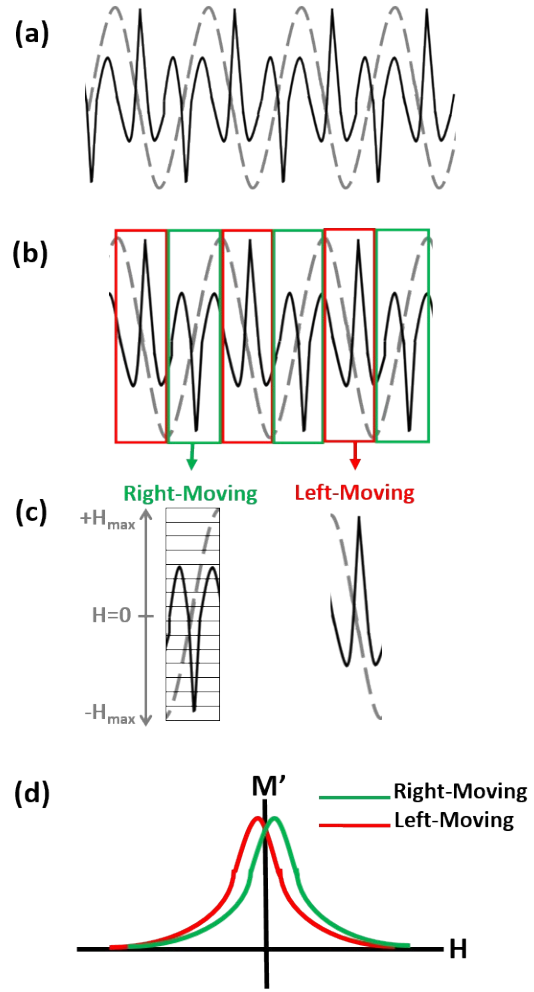


Figure S3. Magnetic relaxometry gridding and PSF reconstruction. The relaxometer's excitation field magnetically excites the sample and induces magnetization reversal, which is equivalent to one-dimensional FFR movement across the sample. The raw MPI signal (black solid line) is inductively received and amplified using a low-noise preamplifier (SRS 560), and the known excitation field (gray dotted line) is reconstructed (a). The raw signal and instantaneous excitation field are split into left-moving and right-moving components (defined by the derivative of the excitation field, also known as FFR velocity; a positive derivative corresponds to right-moving FFR) (b). Each signal component is binned according to instantaneous excitation field value, and averaged by number of samples per bin (c). The averaged bin values are then gridded to instantaneous excitation field value to generate the PSF (d).

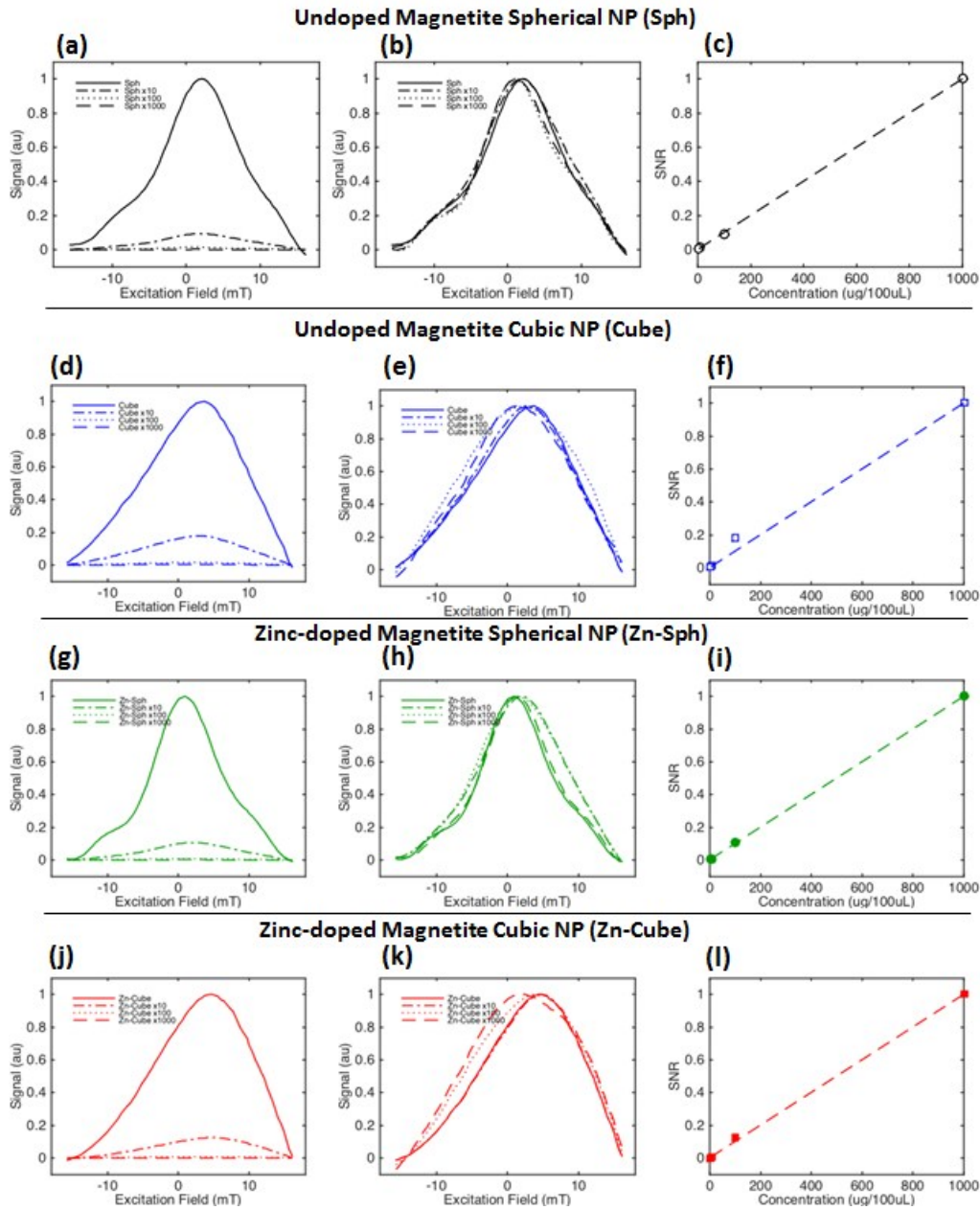


Figure S4. The PSF of magnetite spherical NP, magnetite cubic NP, zinc-doped magnetite spherical NP and zinc-doped magnetite cubic NP normalized to signals obtained from 1 mg Fe (a, d, g, j). The corresponding PSF normalized to the peak value of individual concentration PSF (b, e, h, k). The corresponding SNR vs. concentration (c, f, l, i).

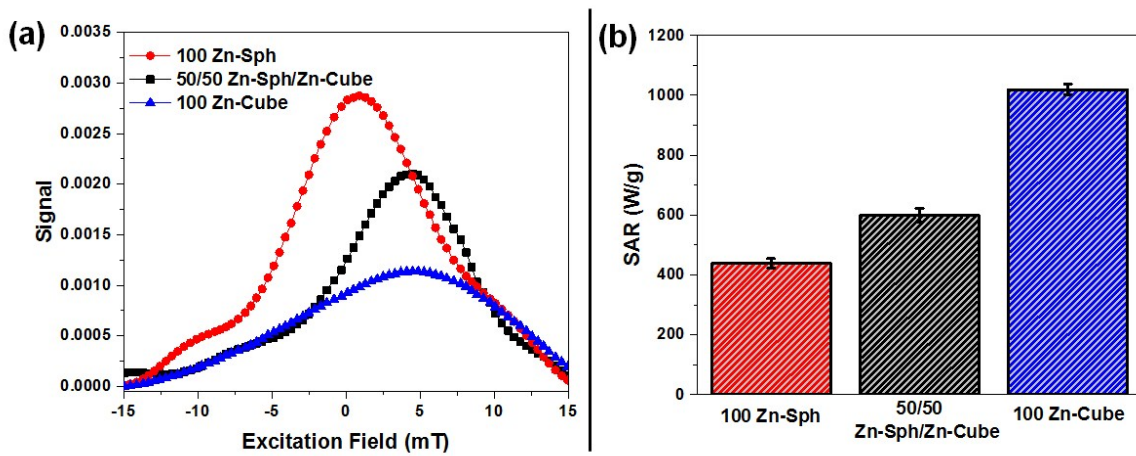


Figure S5. The point spread function (PSF) (a) and the specific absorption rate (SAR) values (b) of the 100 % Zn-Sph, 50/50 % Zn-Sph/Zn-Cube and 100 % Zn-Cube IONP samples.

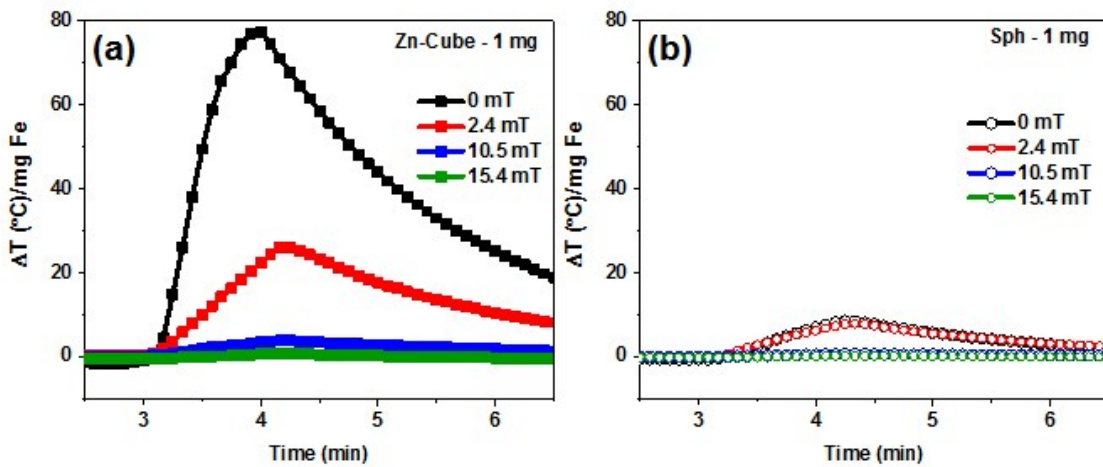


Figure S6. Temperature profiles of zinc-doped magnetite cubic NP ($\text{Zn}_{0.4}\text{Fe}_{2.6}\text{O}_4$, Zn-Cube) (a), and magnetite spherical NP (Fe_3O_4 , Sph) (b) during magnetic hyperthermia measurements under external static magnetic field at 0, 2.4, 10.5 and 15.4 mT.

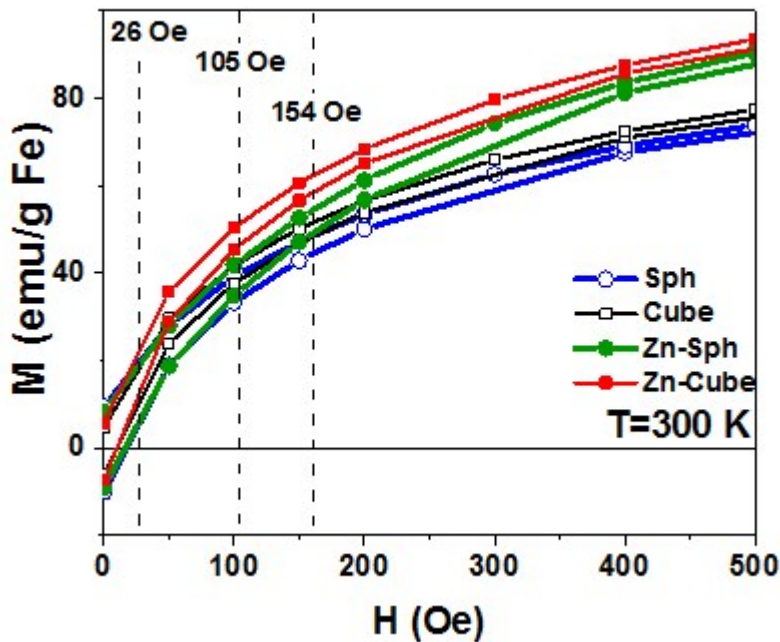


Figure S7. The upper right quadrant of the field-dependent hysteresis curves of Sph, Cube, Zn-Sph and Zn-Cube nanoparticles. The strengths of the static field are represented in the dotted lines.

References

1. J. Park, K. An, Y. Hwang, J.-G. Park, H.-J. Noh, J.-Y. Kim, J.-H. Park, N.-M. Hwang and T. Hyeon, *Nat. Mater.*, **2004**, *3*, 891–895.
2. D. Kim, N. Lee, M. Park, B.H. Kim, K. An and H. T. Hyeon, *J. Am. Chem. Soc.*, **2008**, *131*, 454-455.
3. J. Jang, N. Nah, J.-H. Lee, S.H. Moon, M.G. Kim and J. Cheon, *Angew. Chem. Int. Ed.* **2009**, *48*, 1234-1238.
S. H. Noh, W. Na, J. T. Jang, J. H. Lee, E. J. Lee, S. H. Moon, Y. Lim, J. S. Shin and J. Cheon, *Nano Lett.*, **2012**, *12*, 3716–3721.